The Journal of Chemical Physics

The coexistence curve and surface tension of a monatomic water model

Cite as: J. Chem. Phys. **156**, 154505 (2022); https://doi.org/10.1063/5.0085252
Submitted: 14 January 2022 • Accepted: 18 March 2022 • Published Online: 19 April 2022

Mary K. Coe, Robert Evans and Nigel B. Wilding

The Journal of Chemical Physics ARTICLE scitation.org/journal/jcp

The coexistence curve and surface tension of a monatomic water model

Cite as: J. Chem. Phys. 156, 154505 (2022); doi: 10.1063/5.0085252
Submitted: 14 January 2022 • Accepted: 18 March 2022 •
Published Online: 19 April 2022

Mary K. Coe, Robert Evans, and Nigel B. Wilding[a)]

AFFILIATIONS

H.H. Wills Physics Laboratory, University of Bristol, Bristol BS8 1TL, United Kingdom

[a)]Author to whom correspondence should be addressed: nigel.wilding@bristol.ac.uk

ABSTRACT

We study the monatomic water model of Molinero and Moore the grand canonical ensemble Monte Carlo simulation. Measurements of the probability distribution of the number density obtained via multicanonical sampling and histogram reweighting provide accurate estimates of the temperature dependence of both the liquid–vapor coexistence densities and the surface tension. Using finite-size scaling methods, we locate the liquid–vapor critical point at $T_c = 917.6$ K, $\rho_c = 0.311$ g cm^{-3}. When plotted in scaled variables, in order to test the law of corresponding states, the coexistence curve of monatomic water is close to that of real water. In this respect, it performs better than extended simple point charge (SPC/E), TIP4P, and TIP4P/2005 water.

I. INTRODUCTION

Monatomic water (mw)[1] is a relatively new water model. While more established models, such as SPC/E,[2] TIP4P,[3] and TIP4P/2005,[4] seek to accurately describe the molecular structure of water, mw instead represents water as a single atom. In addition, it dispenses with the long-ranged electrostatic interactions of the more sophisticated models, instead reproducing the tetrahedral structure of water using a short-ranged three-body interaction which favors tetrahedral coordination. Short-ranged pair interactions between mw atoms remain, much like those between oxygen atoms in atomistic models of water. By using only short-ranged interactions and a single atom, mw has been found to be over one hundred times faster to implement in simulations than models with long-ranged interactions.[1] This together with the fact that mw at low temperature yields values of the liquid–vapor surface tension, density, enthalpy of vaporization, and melting temperature[1,5] that are in many cases closer to those of real water than atomistically more detailed models, means that mw has great promise as a realistic and efficient water model.

The mw model has proven popular in a variety of contexts such as for studies of hydrophobicity.[5–7] However, phase properties above ambient temperature have not been explored in detail. In the present work, we address this by measuring, to high accuracy, the liquid–vapor binodal (coexistence) curve and the location of the critical point of mw. We also determine the temperature dependence of the surface tension. We compare our results with those for the SPC/E, TIP4P, and TIP4P/2005 models and with experimental data for water.

II. MODEL AND METHODS

A. Description of mw model

mw is based on a re-parameterization of the well-known Stillinger–Weber potential, which was used originally to model elements such as silicon and germanium that exhibit similar tetrahedral structures to that of water. Molinero and Moore chose to parameterize mw to reproduce the melting temperature, vaporization enthalpy, and density of water at ambient conditions. Based on this parameterization, the form of the interaction potential is[1]

$$\phi_{mw}(\mathbf{r}_i, \mathbf{r}_j, \mathbf{r}_k, \theta_{ijk}) = \sum_i \sum_{j>i} \phi_{mw,2}(\mathbf{r}_i, \mathbf{r}_j) + \sum_i \sum_{j\neq i} \sum_{k>j} \phi_{mw,3}(\mathbf{r}_i, \mathbf{r}_j, \mathbf{r}_k, \theta_{ijk}), \quad (1)$$

where the two-body, $\phi_{mw,2}$, and three-body, $\phi_{mw,3}$, potentials are

$$\phi_{mw,2}(\mathbf{r}_i,\mathbf{r}_j) = A\varepsilon_{mw}\left[B\left(\frac{\sigma_{mw}}{r}\right)^4 - 1\right]\exp\left(\frac{\sigma_{mw}}{|\mathbf{r}_i-\mathbf{r}_j| - a\sigma_{mw}}\right), \quad (2)$$

$$\begin{aligned}\phi_{mw,3}(\mathbf{r}_i,\mathbf{r}_j,\mathbf{r}_k,\theta_{ijk}) = {} & \lambda\varepsilon_{mw}\left[\cos\,\theta_{ijk} - \cos\,\theta_0\right]^2 \\ & \times \exp\left(\frac{\gamma\sigma_{mw}}{|\mathbf{r}_i-\mathbf{r}_j| - a\sigma_{mw}}\right) \\ & \times \exp\left(\frac{\gamma\sigma_{mw}}{|\mathbf{r}_i-\mathbf{r}_k| - a\sigma_{mw}}\right), \end{aligned} \quad (3)$$

and $A = 7.049\,556\,277$, $B = 0.602\,224\,558\,4$, and $\gamma = 1.2$ are constants that determine the form and scale of the potential, $\lambda = 23.15$ is the tetrahedrality parameter, $\theta_0 = 109.47^\circ$ is the angle favored between waters, $a = 1.8$ is the inverse cut-off radius, $\sigma_{mw} = 2.3925$ Å is the diameter of a mw particle, and $\varepsilon_{mw} = 6.189$ kcal mol^{-1} is the mw–mw interaction strength.

B. Simulation ensemble, observables, and sampling methods

Our study is conducted in the grand canonical ensemble (GCE).[8] The GCE is widely acknowledged to be the most accurate and flexible when it comes to determining fluid coexistence properties because it allows for fluctuations of the order parameter on the scale of the system size. Our approach follows closely that of a previous study of the truncated Lennard-Jones fluid.[9] Specifically, we perform measurements of the joint probability distribution $P(\rho,u)$ of the number density $\rho = N/V$ and the energy density $u = U/V$, where $V = L^3$ is the system volume. This distribution, accumulated as a histogram, is obtained in the coexistence region with the aid of "Multicanonical" sampling[10] and histogram reweighting techniques.[11]

The multicanonical method is a biased sampling method that allows both vapor and liquid pure phase states to be sampled in a single simulation. It does so by using a weight function to remove the sampling barrier associated with mixed phase states that needs to be traversed for the simulation to pass between the pure phase states. In the process, the method provides an estimate of the relative probability of pure phase and mixed phase states, which in turn allows an estimate of the liquid–vapor surface tension as described below.

In practice, the multicanonical weight function is defined with respect to an order parameter chosen to distinguish between pure and mixed phase states. For the purpose of constructing a sampling path between vapor and liquid, we assign the order parameter to be the particle number density ρ so that the weight function is $\eta(\rho)$. The Monte Carlo simulation then operates with an effective Hamiltonian $\mathscr{H}' = \mathscr{H} + \eta(\rho)$, where $\mathscr{H} = \phi_{mw} - \mu N$ is the grand canonical Hamiltonian. The standard grand canonical Monte Carlo acceptance probabilities[8] are modified to read

$$\begin{aligned} P_{acc}(N \to N+1) &= \min\left[1, \frac{V}{(N+1)}e^{-\beta(\Delta\phi_{mw}-\mu)+(\eta(N+1)-\eta(N))}\right], \\ P_{acc}(N-1 \to N) &= \min\left[1, \frac{N}{V}e^{-\beta(\Delta\phi_{mw}+\mu)+(\eta(N-1)-\eta(N))}\right]. \end{aligned} \quad (4)$$

The multicanonical sampling yields a measure of the biased probability distribution $P'(\rho,u)$. This is simply related to the true equilibrium distribution via

$$P'(\rho,u) = P(\rho,u)e^{\eta(\rho)}. \quad (5)$$

Provided that $\eta(\rho)$ is chosen such that $P'(\rho) \approx$ constant, it allows for barrier free sampling of $P'(\rho,u)$ over the whole range of ρ spanning the pure phase states. The requisite form of $P(\rho,u)$ is subsequently found by inverting Eq. (5). As Eq. (5) shows, the form of $\eta(\rho)$ that yields $P'(\rho,u) \approx$ constant is $\eta(\rho) \approx -\ln P(\rho)$. Since $P(\rho)$ is just the function we seek, there is a degree of circularity to the process of determining a suitable weight function. However, robust methods exist for doings so and have been described in detail elsewhere.[12,13]

Histogram reweighting is a well known technique for extrapolating simulation data obtained at one set of thermodynamic field parameters to a nearby set. It achieves this via a reweighting of the Boltzmann probability distribution.[8,11] The technique can be used to synthesize data collected at different state points to allow interpolation as well as extrapolation.[14] Histogram reweighting is invaluable in helping to trace a coexistence curve and for estimating the weight functions required by multicanonical sampling. Using histogram reweighting in combination with multicanonical sampling, it is possible to trace the entire liquid–vapor bulk coexistence curve using only a few simulations.[12]

III. RESULTS

A. Location of the liquid–vapor critical point

While the critical temperature, T_c, of mw has been mentioned in previous studies,[5,15] it is unclear whether these took into account the strong finite-size effects that can affect the critical region. Any simulation performed near the critical point will be subject to finite-size effects due to the divergence of the correlation length, ξ. This means that the apparent values of T_c and the critical chemical potential μ_c observed in a system of finite-size depend on the linear dimension L of the system. In order to determine the true (infinite volume) critical parameters, it is necessary that these finite-size effects are taken into account. This can be achieved by using universal scaling relations to extrapolate the apparent critical parameters obtained from systems of various L to the thermodynamic limit, as described by Wilding.[9] Water and water models have the same essential symmetries as the three dimensional Ising model and are, therefore, expected to belong to the Ising universality class and share the same set of critical exponents.

Within our approach, the apparent critical point parameters $T_c(L)$ and $\mu_c(L)$ are determined by finding, for the prescribed L, the values of μ, T, and s for which the probability distribution of the scaling variable,[9,16] $\mathscr{M} = \rho - su$, best matches the known universal Ising form.[17] Here, s is a mixing parameter, which physically measures the degree of "field mixing,"[16,18] i.e., the extent to which critical fluctuations in the number and energy densities couple. Operationally, s is estimated by tuning its value together with μ and T to affect the best match. Performing this matching also yields a value for the apparent critical density $\rho_c(L)$. Figure 1 shows the quality of the matching for mW using the five values of L that we have considered. In each case, the matching shown was achieved for a value of the mixing parameter, $s \approx 0.33$. This agrees well with the

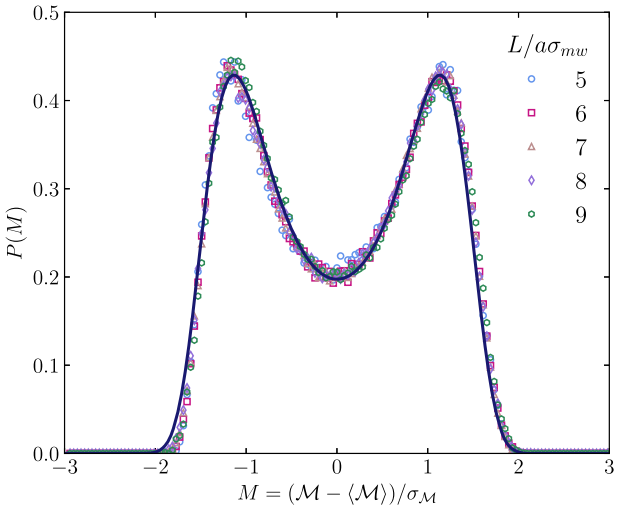

FIG. 1. The probability distribution function of the scaling variable M for mw, measured for various linear system sizes L (expressed in units of $a\sigma_{mw}$) as shown in the key. In addition, shown is the limiting universal Ising distribution (solid line).[17] In each case, the abscissa is scaled to the unit variance by dividing by the standard deviation of the probability distribution.

value quoted by Russo *et al.*[15] in their supplementary information, although their value was related to a weaker value of the tetrahedrality parameter, λ, than we used in mw. Importantly, the sign of s is opposite to that found in the case of the Lennard-Jones fluid[9] (where the value of $s = -0.11$) and to that of other models described solely by pair potentials.[19–21] Our present findings may, therefore, point to a strong influence of three body forces on scaling field mixing in line with previous suggestions.[22,23] We also note that in mw, the apparent critical temperature $T_c(L)$ decreases with increasing L (see Fig. 2) but increases with L in models with solely pairwise interactions. This difference suggests that three body interactions may qualitatively affect the manner in which corrections to scaling contribute to the order parameter distribution.

Figure 2 shows the extrapolation to the thermodynamic limit of the values of $T_c(L)$, $\mu_c(L)$, and $\rho_c(L)$ that were obtained for each L via the matching to the Ising form. The extrapolation uses the expected universal finite-size scaling relationships[9] that describe the L dependence of the apparent critical temperature. This L dependence takes the form of a power law[9] involving the system dimensionality d, the critical correlation length exponent ν, and the critical correction to scaling exponent θ. For the case of T_c in Fig. 2(a), there is excellent agreement, as the linear fit (dotted line) indicates. The extrapolation to $L = \infty$ yields a critical temperature of $T_c = 917.6(10)$ K. This is to be compared with the value of $T_c \approx 925$ K quoted by Xu and Molinero,[5] who did not perform a finite-size scaling analysis. Figure 2(b) shows the corresponding scaling of estimates of $\mu_c(L)$, whose extrapolation to $L = \infty$ yields $\beta\mu_c = -5.110(3)$. Finally, Fig. 2(c) shows the scaling of $\rho_c(L)$. Again, excellent agreement with the predicted scaling relation is found with the extrapolation to $L = \infty$ yielding a critical density of $\rho_c = 0.311(3)$ g cm^{-3}. The critical exponents required for the scaling analysis are given in the caption to Fig. 2.

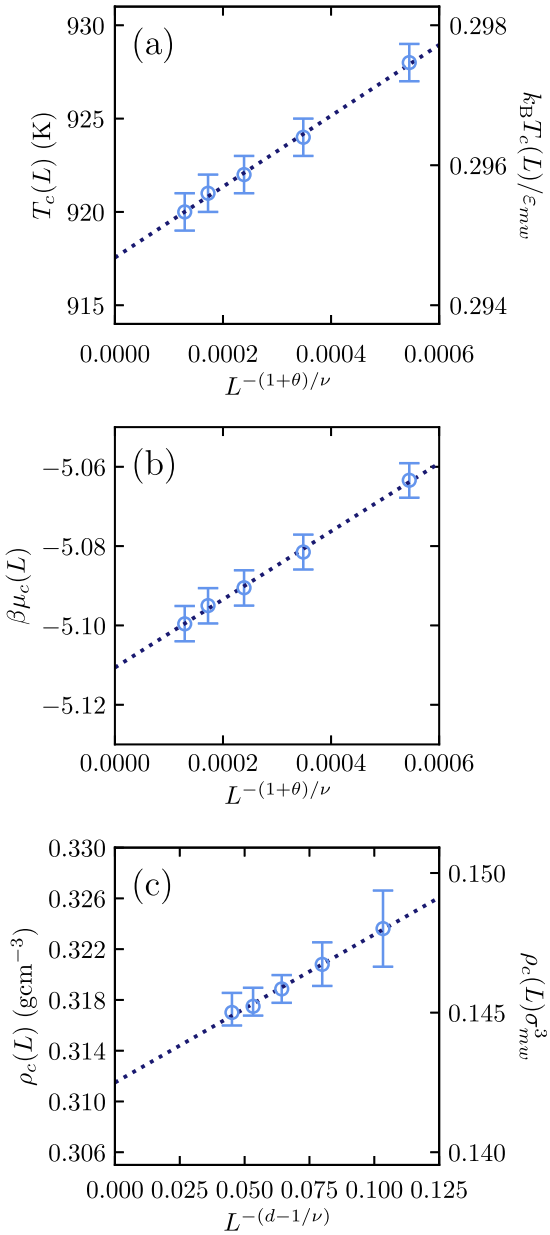

FIG. 2. Finite-size scaling analysis of the critical (a) temperature, (b) chemical potential, and (c) density of mw, in both physical and reduced units. Uncertainties in (a) are taken to be 1 K, while in (c), the uncertainty is obtained from the densities measured at the upper and lower values of the critical temperatures (see error bars) obtained from (a). The exponents were assigned the values[9] $\theta = 0.54$, $\nu = 0.629$, and $d = 3$. σ_{mw} and ε_{mw} are defined in Sec. II A.

Table I compares the critical temperature and density of mw obtained here to the values for SPC/E,[25] TIP4P,[25] TIP4P/2005,[25] and real water.[24] The critical temperature of mw is clearly much larger than that of atomistic water models or real water. This is due to the bond directional entropy of the atomistically more detailed models

TABLE I. The critical temperature and density for water,[24] the SPC/E model,[25] TIP4P,[25] TIP4P/2005,[25] and mw (this work).

Model	T_c (K)	ρ_c (g cm^{-3})
Water	647.096	0.322
SPC/E	638.6	0.273
TIP4P	588	0.315
TIP4P/2005	640	0.31
Mw	917.6(10)	0.311(3)

driving down the critical temperature. However, the critical density of mw is in very good agreement with that of water. The agreement is at a level similar to that of TIP4P and TIP4P/2005 and is much closer than that of SPC/E.

B. Liquid–vapor binodal: Comparison with SPC/E, TIP4P, TIP4P/2005, and experimental water data

Liquid–vapor coexistence state points for mw have been reported previously;[26,27] however, these studies have generally focused on near ambient conditions. Here, we determine mw's wider coexistence properties, ranging from ambient conditions up to the critical temperature.

We have utilized multicanonical sampling and histogram reweighting to determine accurately the coexistence curve $\mu_{co}(T)$ together with the corresponding liquid and vapor densities ρ_l and ρ_v. Close to liquid–vapor coexistence, the probability distribution of the density distribution $P(\rho)$ collected during a Grand Canonical Monte Carlo (GCMC) simulation features two peaks corresponding to the vapor and liquid phases. The exact coexistence conditions, i.e., equal pressure and chemical potential in the two phases, correspond to the areas under each peak being equal.[9] One can then read off the coexistence densities from the peak positions in $P(\rho)$, e.g., by fitting a Gaussian to each peak. Figure 3 shows our results for the coexistence curve of mw in the ρ–T and $\beta\mu$–T planes. A table listing values of the coexisting densities and chemical potential is given in the Appendix.

Figure 4(a) compares the liquid–vapor coexistence curve of mw with that of water, SPC/E, TIP4P, and TIP4P/2005 models, in physical units. Given the large value of T_c, the liquid–vapor phase diagram of mw extends over a much greater temperature range than that of real water and the atomistically detailed models. Despite this, Fig. 4(a) shows that mw reproduces the coexisting liquid density of water fairly well for $T < 400$K. Below 350K, the agreement is similar to that of the atomistically more detailed models, which indicates that, in terms of coexistence properties, mw is a good alternative to these models under near ambient conditions. However, above 400K, mw overestimates the coexistence density of water. This is most severe when $T > 420$K and suggests, at first sight, that away from ambient conditions, mw is a poor model of water.

It is important not to jump to conclusions. The excellent agreement between the critical density of water and mw suggests that mw might better reproduce the phase properties of water if both T and ρ were scaled by their critical values. This is tested in Fig. 4(b). The resulting agreement between the scaled coexistence curves of mw and real water is remarkable and is far better than that between real water and SPC/E and appreciably better than between real water, TIP4P, and TIP4P/2005. Although small differences between the coexistence curves of water and mw can be seen close to the bulk critical point, these may be partially due to finite-size effects. Further study is required to examine the near-critical coexistence region more closely.

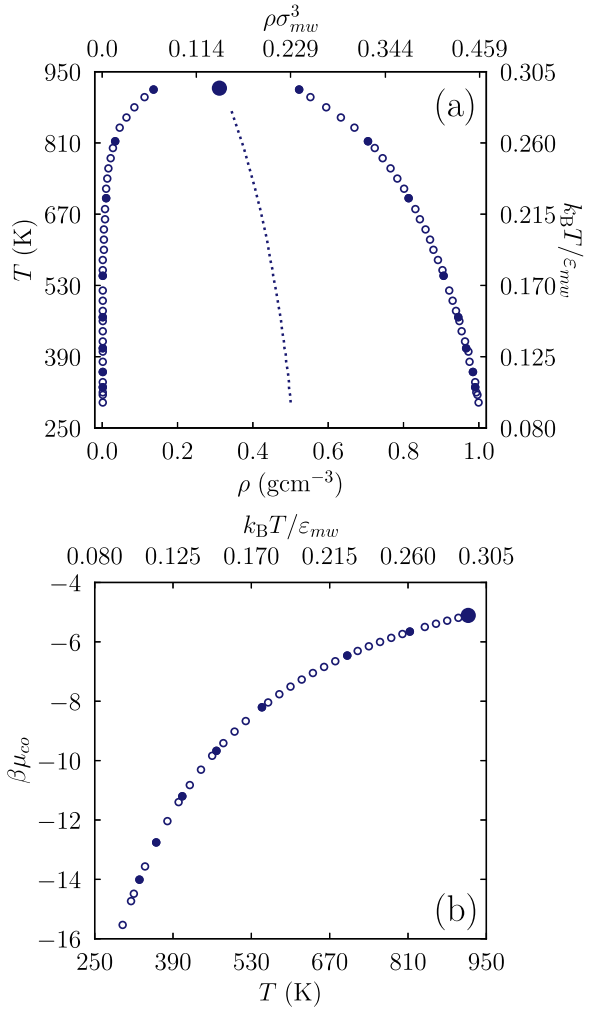

FIG. 3. (a) Results for the liquid–vapor binodal of mw water. Filled circles show the temperature for which GCMC simulations were performed. Unfilled data points were obtained by histogram extrapolation. The critical point is marked by the large filled circle. The dotted line shows the coexistence diameter $\rho_d(T) = (\rho_v(T) + \rho_l(T))/2$. (b) Results for the liquid–vapor coexistence curve in the $\beta\mu$–T plane with $\beta = 1/k_BT$. Symbols are as in (a). A table listing values of the coexisting densities and chemical potential is given in the Appendix. Note also the conversion to reduced units on pertinent axes.

C. Liquid–vapor surface tension: Comparison with SPC/E, TIP4P, TIP4P/2005, and experimental water data

In addition to accounting for the thermodynamic properties of bulk water, a computational model for use in the study of

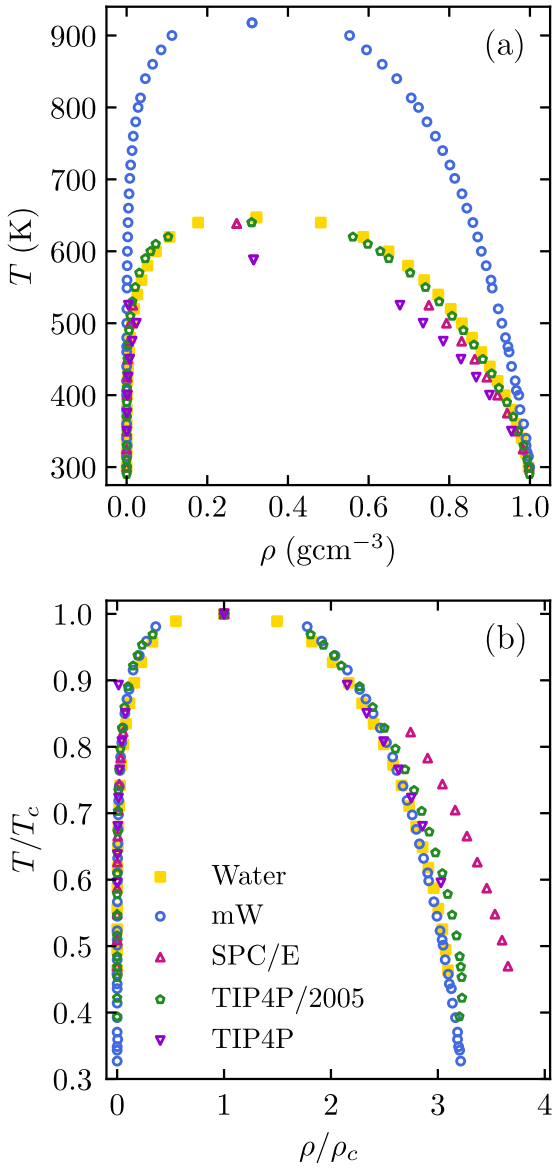

FIG. 4. Liquid–vapor phase diagram for mw (blue circles), SPC/E[28] (pink upward triangles), TIP4P[28] (purple downward triangles), TIP4P/2005[29] (green pentagons), and water[24] (yellow squares) in (a) physical units and (b) in terms of reduced variables, i.e., scaled by their critical values.

interfacial phenomena such as wetting[31] and drying transitions[32] should provide a good description of the liquid–vapor surface tension. Molinero and Moore[1] have previously shown that mw under ambient conditions has a surface tension closer to that of water than SPC/E or TIP4P, and it was noted by Xu and Molinero[5] that mw almost exactly reproduces the surface tension of water at 360 K. Investigation of the behavior of the surface tension of mw over its entire liquid–vapor coexistence range is, therefore, of interest.

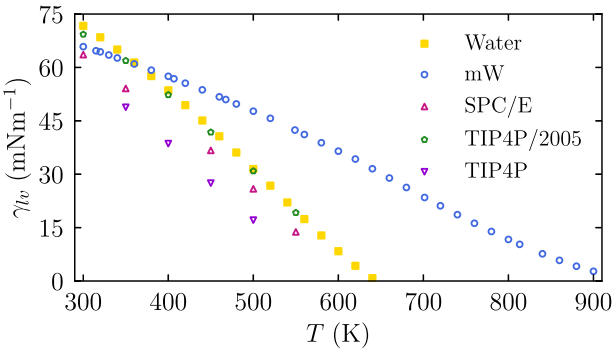

FIG. 5. Comparison of the liquid–vapor surface tension of mw (circles) with SPC/E[30] (pink upward triangles), TIP4P[30] (purple downward triangles), TIP4P/2005[30] (green pentagons), and water[24] (yellow squares).

The liquid–vapor surface tension can be determined from the form of the probability distribution $P(\rho)$ at each coexistence state point in Fig. 4, using[33–35]

$$\gamma_{lv} = \left(\frac{1}{2\beta L^2}\right) \ln\left(\frac{P_{\max}}{P_{\min}}\right), \tag{6}$$

where L is the side length of a cubic simulation box, $P_{\max}$ is the maximum probability within the distribution, which will correspond to both the vapor and liquid peaks, and $P_{\min}$ is the minimum of the density distribution, which occurs between the liquid and vapor peaks and corresponds to mixed phase states. Figure 5 shows the surface tension values obtained for mw (also tabulated in the Appendix), along with literature values for SPC/E, TIP4P, TIP4P/2005, and water.

In agreement with the findings of Molinero and Moore,[1] Fig. 5 shows that the surface tension of mw is closer to that of water than SPC/E under ambient conditions, although TIP4P/2005 water provides even better agreement. Similarly, in agreement with Xu and Molinero,[5] the surface tensions of mw and water also appear near identical at 360K. For higher temperatures still, TIP4P/2005 provides a good agreement with experimental values, while SPC/E and mw fail quite badly. mw's much higher critical temperature makes comparisons difficult; whereas for the bulk coexistence curve, there is an obvious law of corresponding states comparison to be made, there is no clear-cut choice of reduced variables for the surface tension. Examining near critical scaling behavior is of interest, but finite-size effects limit what can be ascertained. More pertinent is the form of the surface tension at lower temperatures where we note that our results for mw exhibit a feature similar to real water. In common with some other associating liquids, water displays a large surface tension and exhibits temperature variation different from that in simple liquids. Specifically, real water has a maximum in the (negative) temperature derivative of the tension at about 470K.[36] Our mw results display a similar feature, albeit at a higher temperature of ~640 K, in keeping with mw's much higher critical temperature.

IV. CONCLUSIONS

Near ambient conditions, mw is an excellent model for the study of water properties. It performs as well as SPC/E, TIP4P,

and TIP4P/2005 in reproducing the density of water in the liquid branch of the coexistence curve below 350 K and fares better than SPC/E in reproducing the surface tension of water below ~400 K. As mw utilizes only short-ranged interactions and coarse grains a water molecule into a single particle, it is far more computationally efficient than models that include charges, i.e., Coulomb interactions.

Away from ambient conditions, mw does not reproduce the properties of water as well as the more detailed models. In particular, mw exhibits a much higher critical temperature than water and as a consequence, above ~400 K, mw overestimates the surface tension. However, when the phase diagrams of mw, SPC/E, TIP4P, TIP4P/2005, and water are all scaled by their critical temperatures and critical densities, mw shows better agreement with water than

TABLE II. GCMC results for the temperature dependence of the reduced coexistence chemical potential $\beta\mu_{co}(T)$, the coexistence vapor density $\rho_v(T)$ and liquid density $\rho_l(T)$, and the liquid–vapor surface tension $\gamma_{lv}(T)$. The final two columns show the uncertainty on the coexistence densities at the temperatures at which simulation were conducted (other data points are obtained by histogram extrapolation). These uncertainties are calculated from the standard error in the estimate of the mean density of the individual peaks in $P(\rho)$. Note that at low T, the vapor density can correspond to only a handful of particles in the system, while the liquid comprises thousands. This disparity can affect the accuracy of measurements of ρ_v. To deal with this, and having established μ_{co} at each T via the equal peak weight criterion for $p(\rho)$, we conduct separate simulations for a much larger system size in which the sampling is constrained to remain in the vapor phase. These separate simulations provide accurate measurements of ρ_v, which are those reported in the table. At temperatures 330 K and below, it was impossible to simulate a system with an adequate number of particles to fit a Gaussian to the vapor peak due to the size required. In these cases, the vapor density was taken to be the arithmetic mean of the density. We note that at low temperature where the vapor behaves as a near-ideal gas, our results can be compared to, and are consistent with, previous vapor pressure measurements for mw.[26]

T (K)	T/T_c	ρ_v (g cm^{-3})	ρ_l (g cm^{-3})	μ_{co}/k_BT	γ_{lv} (mN/m)	σ_l	σ_v
900.00	0.9814	0.112 367 68	0.552 848 99	−5.190 859 77	2.7275		
880.00	0.9596	0.085 399 44	0.594 799 59	−5.287 913 23	4.1511		
860.00	0.9377	0.064 424 14	0.633 753 72	−5.390 490 71	5.8003		
840.00	0.9159	0.046 445 31	0.669 711 37	−5.499 092 91	7.6400		
813.23	0.8867	0.034 459 42	0.705 669 03	−5.654 699 34	10.3001	0.000 079 39	0.000 056 59
800.00	0.8723	0.028 466 48	0.723 647 86	−5.736 255 59	11.6765		
780.00	0.8505	0.022 473 54	0.744 623 16	−5.865 950 73	13.9077		
760.00	0.8287	0.016 480 59	0.765 598 46	−6.003 887 22	16.2231		
740.00	0.8069	0.013 484 12	0.783 577 29	−6.150 682 17	18.6422		
720.00	0.7851	0.010 043 73	0.801 556 12	−6.307 294 67	21.1338		0.000 003 88
701.41	0.7648	0.007 935 10	0.813 542 01	−6.462 356 58	23.4635	0.000 093 80	0.000 003 32
680.00	0.7415	0.006 048 43	0.831 520 83	−6.653 260 73	26.2765		0.000 002 73
660.00	0.7197	0.004 605 69	0.843 506 72	−6.844 693 86	28.9373		0.000 002 31
640.00	0.6979	0.003 495 88	0.858 489 08	−7.050 045 21	31.5454		0.000 001 92
620.00	0.6760	0.002 645 32	0.870 474 96	−7.270 776 49	34.2621		0.000 001 05
600.00	0.6542	0.001 943 02	0.879 464 38	−7.508 142 13	36.4794		0.000 000 87
580.00	0.6324	0.001 435 81	0.891 450 26	−7.764 398 31	38.8508		0.000 000 39
560.00	0.6106	0.001 033 51	0.903 436 15	−8.041 460 70	41.1574		0.000 000 33
548.93	0.5985	0.000 853 16	0.906 432 62	−8.204 646 82	42.4065	0.000 087 59	0.000 000 34
520.00	0.5670	0.000 506 35	0.921 414 98	−8.668 079 51	45.7034		0.000 000 22
500.00	0.5452	0.000 339 88	0.930 404 39	−9.023 509 32	47.7113		0.000 000 17
480.00	0.5234	0.000 219 47	0.939 393 81	−9.411 913 40	49.7442		0.000 000 09
467.61	0.5093	0.000 166 47	0.945 386 75	−9.671 110 88	50.9889	0.000 143 59	0.000 000 06
460.00	0.5016	0.000 137 70	0.948 383 22	−9.837 797 48	51.7416		0.000 000 06
440.00	0.4798	0.000 084 10	0.954 376 16	−10.306 478 79	53.7063		0.000 000 03
420.00	0.4580	0.000 049 42	0.963 365 58	−10.824 255 94	55.5748		0.000 000 02
406.61	0.4434	0.000 032 08	0.966 362 05	−11.201 885 82	56.8210	0.000 144 31	0.000 000 02
400.00	0.4362	0.000 026 78	0.972 354 99	−11.398 392 55	57.5166		0.000 000 02
380.00	0.4143	0.000 013 65	0.975 351 46	−12.038 586 02	59.2340		0.000 000 01
360.00	0.3925	0.000 006 95	0.984 340 88	−12.756 228 04	60.9838	0.000 224 88	0.000 000 005
340.00	0.3707	0.000 002 86	0.990 333 82	−13.565 355 28	62.6633		0.000 000 003
330.00	0.3598	0.000 018 59	0.990 333 82	−14.009 863 18	63.4959	0.000 241 82	
320.00	0.3489	0.000 001 15	0.993 330 29	−14.483 857 05	64.3864		
315.00	0.3435	0.000 000 90	0.996 326 77	−14.733 271 30	64.6797		
300.00	0.3271	0.000 000 40	0.999 323 24	−15.534 382 83	65.8395		

the other models. This finding suggests that mw can serve as a realistic model of water away from ambient conditions, provided that one works in terms of scaled temperature and density [see Fig. 4(b)]. This observation implies that mw and water obey a law of corresponding states.[37] In contrast, this appears not to be true when comparing water with SPC/E, TIP4P, and TIP4P/2005. In future work, it would be interesting to investigate whether one can identify appropriate reduced quantities that allow for a similar data collapse with respect to the liquid–vapor surface tension of mw and water.

Our accurate determination of the coexistence curve parameters should prove useful for future simulation studies of mw water that require careful specification of the deviation from bulk coexistence, especially those pertaining to ambient water. An important example is the study of the equilibrium properties of water near a hydrophobic substrate or solute particle. Here, the relevant physics is controlled by surface critical phenomena and depends sensitively on the deviation of the chemical potential from its coexistence value.[35]

Finally, we have measured the value of the scaling field mixing parameter s that characterizes the degree to which the fluctuations of number density and energy density couple at criticality. The value of s differs in sign from that measured in fluids interacting solely via pair potentials, indicating that the three-body interactions inherent in mw play an important role in modifying the field mixing, as has been suggested previously on general grounds.[22,23]

ACKNOWLEDGMENTS

This work used the facilities of the Advanced Computing Research Centre, University of Bristol. We thank F. Turci and J. Russo for valuable discussions. R.E. acknowledges Leverhulme Trust Grant No. EM-2020-029\4.

AUTHOR DECLARATIONS

Conflict of Interest

The authors have no conflicts to disclose.

DATA AVAILABILITY

The data that support the findings of this study are available within the article.

APPENDIX: TABLE OF COEXISTENCE DENSITIES AND CHEMICAL POTENTIAL AND LIQUID–VAPOR SURFACE TENSION

Table II gives the GCMC results for the temperature dependence of the reduced coexistence chemical potential $\beta\mu_{co}(T)$, the coexistence vapor density $\rho_v(T)$ and liquid density $\rho_l(T)$, and the liquid–vapor surface tension $\gamma_{lv}(T)$.

REFERENCES

[1] V. Molinero and E. B. Moore, J. Phys. Chem. B **113**, 4008 (2009).
[2] H. J. C. Berendsen, J. R. Grigera, and T. P. Straatsma, J. Phys. Chem. **91**, 6269 (1987).
[3] W. L. Jorgensen, J. Chandrasekhar, and J. D. Madura, J. Chem. Phys. **79**, 926 (1983).
[4] J. L. F. Abascal and C. Vega, J. Chem. Phys. **123**, 234505 (2005).
[5] L. Xu and V. Molinero, J. Phys. Chem. B **114**, 7320 (2010).
[6] B. Song and V. Molinero, J. Chem. Phys. **139**, 054511 (2013).
[7] N. Islam, M. Flint, and S. W. Rick, J. Chem. Phys. **150**, 014502 (2019).
[8] D. Frenkel and B. Smit, *Understanding Molecular Simulation*, 2nd ed. (Academic Press, 2002).
[9] N. B. Wilding, Phys. Rev. E **52**, 602 (1995).
[10] B. A. Berg and T. Neuhaus, Phys. Rev. Lett. **68**, 9 (1992).
[11] A. M. Ferrenberg and R. H. Swendsen, Phys. Rev. Lett. **61**, 2635 (1988).
[12] N. B. Wilding, Am. J. Phys. **69**, 1147 (2001).
[13] G. C. McNeil-Watson and N. B. Wilding, J. Chem. Phys. **124**, 064504 (2006).
[14] A. M. Ferrenberg and R. H. Swendsen, Comput. Phys. **3**, 101 (1989).
[15] J. Russo, K. Akahane, and H. Tanaka, Proc. Natl. Acad. Sci. U. S. A. **115**, E3333 (2018).
[16] N. B. Wilding and A. D. Bruce, J. Phys.: Condens. Matter **4**, 3087 (1992).
[17] M. M. Tsypin and H. W. J. Blöte, Phys. Rev. E **62**, 73 (2000).
[18] A. D. Bruce and N. B. Wilding, Phys. Rev. Lett. **68**, 193 (1992).
[19] M. Martín-Betancourt, J. M. Romero-Enrique, and L. F. Rull, Mol. Phys. **107**, 563 (2009).
[20] E. de Miguel, Phys. Rev. E **55**, 1347 (1997).
[21] J.-M. Caillol, D. Levesque, and J.-J. Weis, J. Chem. Phys. **116**, 10794 (2002).
[22] R. E. Goldstein, A. Parola, N. W. Ashcroft, M. W. Pestak, M. H. W. Chan, J. R. de Bruyn, and D. A. Balzarini, Phys. Rev. Lett. **58**, 41 (1987).
[23] R. E. Goldstein and A. Parola, J. Chem. Phys. **88**, 7059 (1988).
[24] E. W. Lemmon, M. O. McLinden, and D. G. Friend, in *NIST Chemistry WebBook, NIST Standard Reference Database Number 69*, edited by P. J. Linstrom and W. G. Mallard (National Institute of Standards and Technology, Gaithersburg, MD, 2021); accessed 29 June 2021.
[25] C. Vega and J. L. F. Abascal, Phys. Chem. Chem. Phys. **13**, 19663 (2011).
[26] M. H. Factorovich, V. Molinero, and D. A. Scherlis, J. Chem. Phys. **140**, 064111 (2014).
[27] M. H. Factorovich, V. Molinero, and D. A. Scherlis, J. Am. Chem. Soc. **136**, 4508 (2014).
[28] *NIST Standard Simulation Website, NIST Standard Reference Database Number 173*, edited by V. K. Shen, D. W. Siderius, W. P. Krekelberg, and H. W. Hatch (National Institute of Standards and Technology, Gaithersburg, MD, 2021); accessed 29 June 2021.
[29] C. Vega, J. L. F. Abascal, and I. Nezbeda, J. Chem. Phys. **125**, 034503 (2006).
[30] C. Vega and E. de Miguel, J. Chem. Phys. **126**, 154707 (2007).
[31] V. Kumar and J. R. Errington, J. Phys. Chem. C **117**, 23017 (2013).
[32] R. Evans and N. B. Wilding, Phys. Rev. Lett. **115**, 016103 (2015).
[33] K. Binder, Phys. Rev. A **25**, 1699 (1982).
[34] J. R. Errington, Phys. Rev. E **67**, 012102 (2003).
[35] R. Evans, M. C. Stewart, and N. B. Wilding, J. Chem. Phys. **147**, 044701 (2017).
[36] J. S. Rowlinson and B. Widom, *Molecular Theory of Capillarity* (Clarendon Press, Oxford, Oxfordshire, 1982).
[37] E. A. Guggenheim, J. Chem. Phys. **13**, 253 (1945).